GOLD MONOLAYER-PROTECTED CLUSTERS FUNCTIONALIZED WITH PEPTIDIC ANTI-HEMAGGLUTININ PARATOPES

By

Matthew Vann Bryant

Thesis

Submitted to the Faculty of the

Graduate School of Vanderbilt University

in partial fulfillment of the requirements

for the degree of

MASTER OF SCIENCE

In

Chemistry

August, 2014

Nashville, Tennessee

Approved:

Professor David W. Wright

Professor Carmello Rizzo

TABLE OF CONTENTS

Page

LIST OF FIGURES

Page

LIST OF TABLES

Page

LIST OF ABBREVIATIONS

Symbol

HA	hemagglutinin
RBD	receptor-binding domain
CDR	complimentarity determining region
MRE	molecular recognition element
Tio	tiopronin
MPC	monolayer-protected cluster
FMOC	fluorenylmethyloxycarbonyl
TEM	transmission electron microscope
TGA	thermogravimetric analysis
ELISA	Enyme-Linked Immunosorbent Assay
QCM	quartz-crystal microbalance
BLI	bio-layer interferometry
k_f	forward kinetic rate constant
k_r	reverse kinetic rate constant
R	response parameter (shift)
R_{max}	maximum response (shift)
$\frac{d}{dt}$	derivative with respect to time
$[B]_o$	initial concentration of surface immobilized biomolecule

Chapter I

MODULAR ANTI-HEMAGGLUTININ PEPTIDE DEVELOPMENT

Introduction

Influenza is a virus that affects humans most commonly as a seasonal infection. In recent years the population has seen variations of the flu that have a pandemic nature (Avian Flu, Swine Flu, Hong Kong Flu). These pandemic outbreaks have caused numerous amounts of deaths and sparked panic in affected communities. Influenza is a enveloped orthomyxovirus that contains 8 pieces of RNA which encode for 10 proteins, hemagglutinin (HA), neuraminidase (NA), nucleoprotein, two matrix proteins, three viral polymerase proteins, and two nonstructural proteins (Figure 1).[10] The HA protein has been a target of research dedicated to understanding

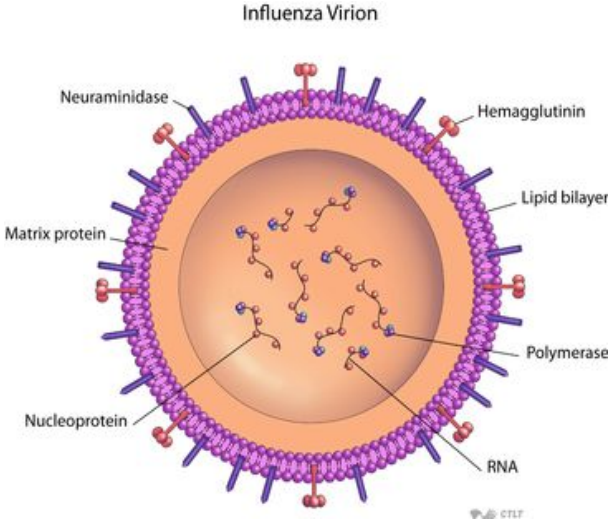

Figure 1. Structure and proteins of the Influenza virion.

the structure and function of this surface protein in the grand scheme of the influenza virus. Within influenza A, there are different sub types of HA proteins found on the virion and they are

labeled numerically 1-17, with 1, 2, and 3 being the most common in human infection.[10] HA is a surface protein that has been designated as the mediator of fusion and infection of epithelial cells. There are three different genera of the influenza virus, A, B, and C. Influenza A is the most common that affects humans. Within influenza A there is only one species and this species is found almost exclusively in aquatic birds. Transmission of the influenza A virus to domestic poultry, and domestic livestock has given rise to the large outbreaks in the human population ex. H1N1 (swine flue), H5N1 (bird flu).[10-12] The combinatory nature of these pandemic influenza viruses is due to the containment of RNA sequences found in bird and pig.

Immunology of Influenza and Anti-Influenza Antibodies

Once exposed to influenza, humans develop antibodies to help neutralize the virus and these antibodies are stored as memory cells. Normally a more severe infection occurs when the human exposed to the virus does not have the correct antibodies stored as memory cells and the virus can infect the host, on-setting rapid decline of health. Current treatment methods and therapeutics consist mostly of vaccination, some antiviral medication, and limited immunotherapy. Vaccinations are available to humans that are a combination of non-infective influenza virus and common strain for that season. Thus, once injected will create an immune response as if infected and create memory cells for neutralization if exposed to the true virus. The vaccinations only work on one specific influenza virus and may not protect one from infection from another strain. Strains that have not been introduced to large amounts of the human population can lead to severe infections and death. Experts think that virus strains that have not been introduced to the population in 50+ years such as H2N2 will be pandemic if circulated.[13, 14] Therefore there is a push for alternative vaccination strategies for these pandemic strains of H2N2 and H3N2. Antibodies against HA can inhibit fusion, by blocking the receptor-binding domain located at the top or *head* of the HA protein. This neutralizes the virus and does

not allow it from attaching to healthy cells. These antibodies that show activity against pandemic strains of influenza are not common in today's population. Therefore valuable information can be obtained by screening anonymous blood donors for antibodies that recognize these types of influenza strains. Currently at Vanderbilt University antibodies are screened, studied and sequenced to determine the basis of their specific reactivity to influenza viruses as well as testing for reactivity with other strains. This can prove to be helpful for treatment and vaccination efforts if the H2N2 or H3N2 strains are reintroduced to the human population. We believe that this epidemiologically, biologically, and chemically relevant information can be coupled with bioinorganic research efforts to create a novel technology such as an antibody-mimic AuMPC.

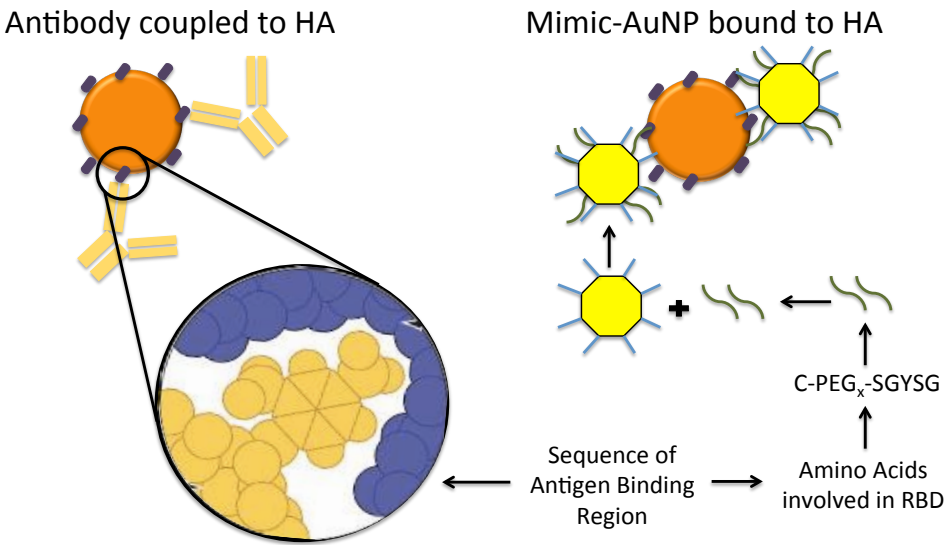

Figure 2. Antibody-antigen schematic contrasting natural antibody binding and synthetic AuMPC binding.

Development of a gold nanoparticle probe that can mimic antibodies against influenza is an appealing alternative to traditional vaccine design. The components of our probe are, the gold nanoparticle as our platform, and a ligand that will be attached to the nanoparticle (Figure 2).

The design of this probe was achieved by understanding the dominant interactions between the antibody and influenza virus. Experimental data from x-ray crystallography and protein

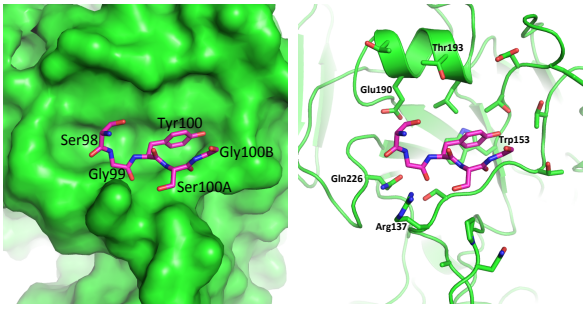

Antibody	CDR-H3 Sequence
8F8	CARQQDSGYSGPEVSYYSHYGMDVW
8M2	CARVGGEWGSGRYYLDHW
2G1	CARGISGSYGWFDPW

Figure 3. X-ray cystal data shown as stick diagram and space filling model of residues 98-100B of antibody 8F8 along with table showing CDR-H3 sequence of all 3 antibodies of interest.

sequencing was the insight into these interactions and the road map by which we will design our probe. We employed a modular or "top down" approach to probe design to incorporate specificity while allowing chemical flexibility such as ligand length and presentation. Gold monolayer protected clusters (AuMPCs) are our platform, and the ligand contain certain chemical aspects of antibodies to the hemagglutinin (HA) surface protein of influenza. The *long-term goal* this work will be to use this antibody biomimetic as a hemagglutination inhibitor (HI) of influenza virus. We hypothesized that a gold nanoparticle antibody biomimetic can be designed as a mimic to the natural antibody-antigen interaction, and the effectiveness can be determined by binding studies using HA.

Inspiration

HA is a homo-trimeric integral membrane glycoprotein that is found on the surface of the influenza virion. The protein's 3-dimensional structure is described as a central α-helix coil ~14 nm long, approximately 80,000 Daltons, and consisting of 3 polypeptides. The heads of these α-helices are used in mediating viral fusion and the hydrophobic portion of the polypeptide is in contact with the viral membrane.[11] The "head" portion of HA binds to the monosaccharide sialic acid present on the membranes of cells; this is characteristic of the surface of epithelial cells of the upper respiratory tract and erythrocytes (red blood cells). The binding of HA to erythrocytes causes them to clump together in a process known as hemagglutination. HA binds to healthy epithelial cells by binding sialic acid causing the virions to stick to the cell surface. The binding of the HA to the cells is called fusion and is the second step in the virus infection after exposure. Work by Hirst determined that the HA was indeed the surface protein responsible for fusion and entrance into cells.[11] The structure of the receptor-binding domain of HA as well as the structure of sialic acid gives important information about their affinity for one another. Sialic acid has numerous alcohol groups stemming from the sugar backbone. The sequencing of the receptor-binding domain of HA shows that there are amino acids that facilitate hydrogen bonding.[11] Therefore, one option for neutralizing the virus is to block the HA from binding to the sialic acid receptors of a healthy cell, this is known as fusion inhibition. Fusion inhibition of the influenza virus is accomplished naturally by the immune response and development of antibodies that bind to the globular head of the HA protein. The binding of an antibody to the head portion occupies the site that would be used for sialic acid binding and cell fusion, thereby neutralizing the virion. Antibodies are a Y-shaped protein produced during an immune response by B-cells to rid the organism of foreign antigens. The immunoglobulin are water-soluble glycoproteins that account for approximately 20% of total protein in serum.[16] The structure of all immunoglobulin consists of two heavy chains and two light chains that are connected through disulfide bonds. There are

conserved and variable regions of immunoglobulin; the variable regions are what give the immunoglobulin specificity for a specific antigen. Within the variable domain of the antigen receptor there are 3 complimentarity determining regions (CDR1, CDR2, and CDR3). The CDR3 associated with the heavy chain of the antibody (CDR-H3), exhibits the highest variability in sequence and is considered *hypervariable*.[16] When designing a peptide to mimic CDRs of an antibody to a specific antigen, having the sequence of the antigenic protein (HA), and the CDR prove to be valuable chemical data. We would like to use this natural antibody-antigen complex as the design basis of our nanoparticle biomimetic.

Currently Dr. Crowe and collaborators are working on analyzing human monoclonal antibodies against influenza viruses. This is done using high-throughput screening of patient samples against the pandemic 1957 H2N2 and the pandemic 1968 H3N2 viruses.[17] These efforts have discovered antibodies that bind and neutralize the HA surface receptor of influenza. This

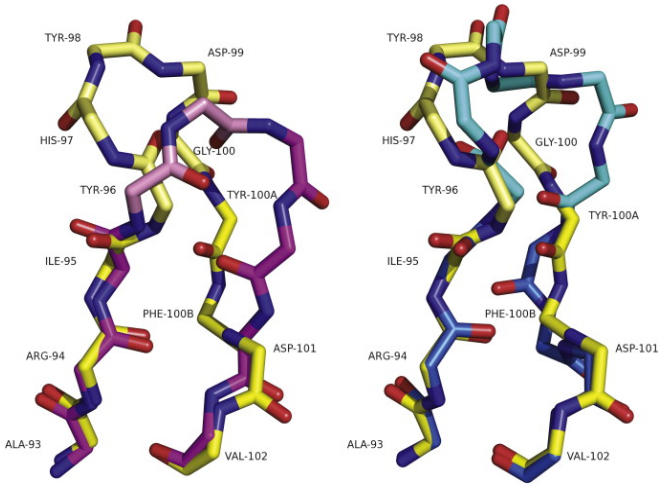

Figure 4. Modeled CDR-H3 conformatons using known structural "anchoring" motifs.[17]

neutralization occurs through binding the HA receptor with the CDR-H3 of the antibodies heavy chain and thereby blocking fusion. More importantly some of the antibodies found have been

shown to have activity across different subtypes of HA receptors (H2/H3), which is very rare.[17] The complexes of the HA protein with three different anti-HA antibodies 8F8, 2G1, 8M2 have been crystallized and the sequences have been mapped (Figure 3).[36]

Mapping of these antibodies has allowed these researchers to determine that the CDR-H3s have amino acids that are found to be in the receptor-binding domain of one of the monomers of HA. HI assays have been done with these antibodies and the data has confirmed that these antibodies specifically bind to the HA protein. These CDR-H3's have been sequenced and the amino acids of these specific antibody prove to be a linear chain that can be easily incorporated into our design (Figure 3). Alternatively, there is work being done to cluster the CDR loop conformations of many antibodies using the inherent conservation of the canonical loop confirmations seen in CDRs. This allows for modeling of unknown CDR-H3 loop sequences using known loop structures by designating anchor regions that are similar across antibodies (Figure 4).[18] The modeling has given researchers a distance associated with the anchoring region of the CDR-H3 and this proved to be valuable information that was used in the planning and design of the modular ligand.

Conclusions

Due to the pandemic nature of influenza strains that the general population has not been exposed to, there is a current need for alternative approaches to fusion inhibition of influenza viruses. We have shown precedence for bringing forward preliminary research utilizing the disciplines of immunology, virology, and inorganic chemistry. The binding assays done with the native antibody gives us confirmation of specificity. The sequencing and structural determination research is paramount, providing the measurements and a picture of the interaction. These insights into the antigen-antibody interaction of these pandemic influenzas

helped to achieve design and synthesis of a gold nanoparticle that mimics the CDR-H3 of an antibody that can bind HA receptors.

CHAPTER II

GOLD MONOLAYER-PROTECTED CLUSTERS FUNCTIONALIZED WITH MODULAR ANTI-HEMAGGLUTININ PEPTIDES

Introduction

Nanobiotechnology utilizing functionalized gold surfaces and gold nanoparticles has been an important research tool for the past twenty years. Gold nanoparticles have been used in a variety of different chemical applications for the last 30 years. They offer discreet size ranges, ability to tune shape, ease of purification, and facile ligand attachment. There is precedence for using gold nanoparticles as a platform for nanoparticle-ligand based immunoassays in the literature and previous work in the Wright lab.[4, 5, 8, 9, 19-24] The field has evolved from synthesis of discreet nanoclusters, to immunogold staining to electron imaging of tissue with gold particles, to quartz-crystal microbalance techniques, and more recently the targeted nanoparticle-ligand binding probes of today.[1-7] A critical component of these probes are the interfaces between the nanoparticle and biological molecules, for it determines both the specificity and sensitivity of these probes. Recently research efforts have focused on the biological efficacy of these nanoclusters when functionalized with proteins, namely antibodies. Successful covalent attachment of antibodies to gold particles has been used for immunoassays and some diagnostics. The antibodies large size (150 kDa) limits the ability to control packing and ease of attachment to such small gold clusters. The Wright lab has used functionalized gold surfaces for

development of diagnostic tools in malaria, detection of explosives, capture and detection of proteins, imaging of RNA in living cells, and presentation of antigenic peptides.[5, 8, 9] These varied tools highlight the breadth of potential applications. Gold nanoparticles can be 'tuned' by size and shape, and considering the ease with which they can be functionalized, are attractive platforms for applications in bioinorganic chemistry. The Murray lab pioneered the AuMPC cluster frontier. They successfully synthesized and characterized different sized AuMPC clusters with numerous types of ligands. The Murray lab was also able to functionalize the particles surface with specific ligands of their choosing using place-exchange reactions. These place-exchange reactions are achieved using thiol-terminated ligands that can replace the original surface ligand and create a covalent-like bond with the surface atoms of the AuMPCs.

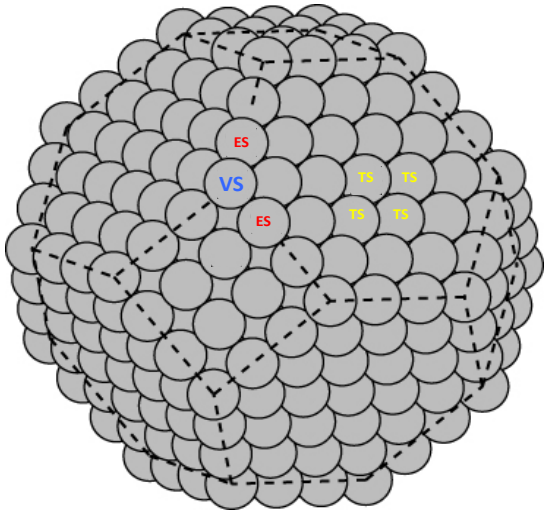

Figure 5. Face-centered cubic truncated octahedron, where the (111) and (100) planes are shown with dotted lines. ES, Edge Sites; VS, Vertex Sites; TS, Terrace Sites.

AuMPCs have previously been used in the Wright lab for epitope presentation of an antigenic HA peptide. This work done by Dr. Gerdon showed that synthesized peptidic epitope

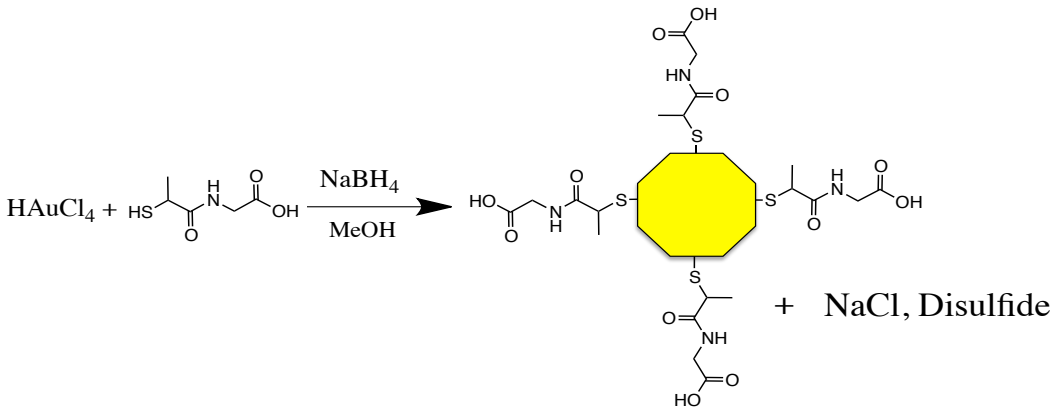

Figure 6. Reaction schematic for tiopronin monolayer-protected cluster synthesis.

sequence AYDPVDYPY of HA could be used to functionalize AuMPCs and 2-D gold surfaces. These epitopes were presented on the gold surface then recognized by an anti-HA antibody using Quartz Crystal Microbalance technology to develop a gravimetric immunoassay. Given this **AuMPC-antigen** biomimetic's ability to be recognized by the antibody, we decide to explore the reverse by making a gold antibody mimic MPC. The original design of the AuMPC biomimetic is a multidisciplinary effort, using techniques in biology, immunology, virology, X-ray crystallography, and inorganic chemistry. The key was incorporating the data compiled by Dr. Crowe, and Dr. Ian Wilson along with the literature precedence for functionalized AuMPC applications. We used 2-3nm Gold tiopronin monolayer-protected clusters (tio-AuMPC). The easy synthesis, fairly monodisperse size-range, and precedence in the Wright lab, afforded us the framework to pursue the research described herein. The structures of tio-AuMPCs have been studied using TEM, and MS.[7, 26, 27] Understanding the structure and shape of these tio-AuMPCs

and how that affects the place exchange and presentation of the ligand on the surface were imperative for probe design. The 2-3 nm tio-AuMPCs will be synthesized using a modified literature basis.[7] These 2-3 nm tio-AuMPCs have the ability to be functionalized with thiolated ligands of choice post-synthesis.[25] The size and shape of gold AUMPCs have been extensively studied by Whetten and coworkers.[28] Nanocrystal gold cores of varying size were studied using mass spectrometry and high-resolution transmission electron microscopy (HR-TEM). Researchers determined the number of atoms along the edge sites of different size nanocrystalline gold cores assuming a face-centered cubic arrangement and truncated octahedron structural motif.[28] The gold atoms at the vertex sites such as the intersection of the (111) and (100) facets are more likely to be involved in the place exchange mechanism due to higher reactivity (Figure 6). The dynamics of the place exchange reaction are more favorable at the vertex sites and edge sites of the cluster.[25] The distance between these vertex sites are determined using the size and structure of the AuMPC. Therefore tuning the AuMPC size and having ligand modularity we can closely mimic the metrics and conformation of the CDR-H3s of interest.

Geometry of Tiopronin Gold Monolayer-protected Clusters

Assuming our AuMPCs are perfect truncated octahedrons we were able to derive a formula for determining the distances on the octahedron faces. The radius *r* of a sphere that touches all points of a regular octahedron (Figure 7), where *x* is the lateral edge length is

$$r = \frac{x}{2}\sqrt{2} \quad \text{(Eq. 1).}$$

Using our AuMPC diameter range 2-3nm we can calculate radii *r* range 1-1.5 nm and edge length *x* range 1.4-1.7 nm respectively.

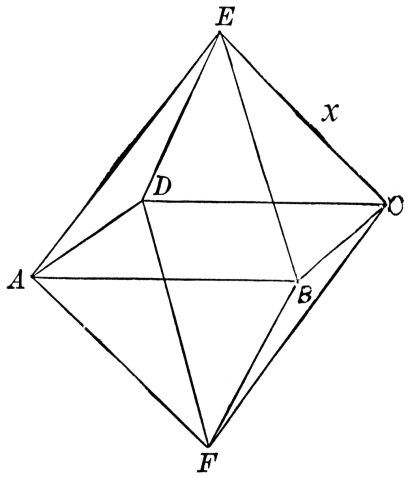

Figure 7. Regular truncated octahedron with equilateral triangular faces, edge length *x* and 6 points (A, B, C, D, E, F).

A truncated octahedron is formed by removal of 6 right square pyramids from each point of a regular octahedron of side length *x*.

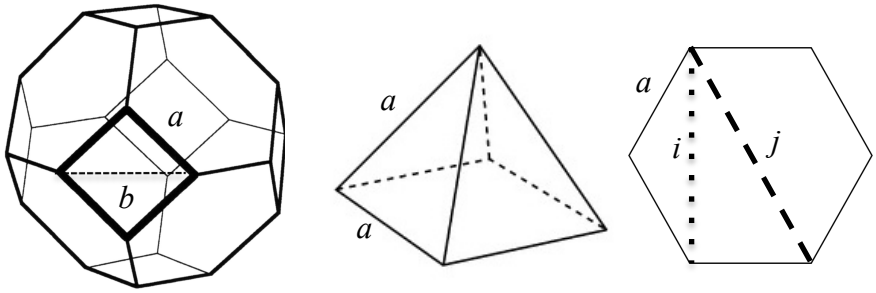

Figure 8. Left, truncated octahedron with square-face length e and square-face vertex-to-vertex length *b*. Middle, right square-pyramid that was removed from each point with base length *a*, and lateral side length a. Right, regular hexagon face with vertex-to-vertex lengths *i* and *j*.

Assuming creation of regular hexagon faces then the equilateral right square pyramids created have pyramid base length *a*, and the pyramid lateral side length *a* where

$$a = \frac{x}{3} \text{ (Eq. 2).}$$

This formula can be used to determine the vertex-to-vertex distance range *a* = 0.46-0.56 nm. Using the definition of a right triangle we can determine the hypotenuse *b* of the right triangle created by the base of the pyramid with

$$\left(\frac{x}{3}\right)^2 + \left(\frac{x}{3}\right)^2 = b^2 \text{ (Eq. 3).}$$

This formula can then be used to determine the hypotenuse *b*, which affords us vertex-to-vertex distance range *b* = 0.66-0.8 nm. The other vertex-to-vertex distance ranges on the hexagonal face labeled *i*, and *j* can be calculated using the same principles and afford us *i* = 0.8-0.98 nm and *j* = 0.92-1.12 nm. Our 2-3 nm AuMPC has 4 distinct vertex-to-vertex distance ranges *a*, *b*, *i*, and *j* (Table 1). If we assume the peptide loop formed has a circular shape, we can determine the length of the semicircle with diameter *b*, as it relates directly to the vertex sites. Using calculated value ranges of *a*, *b*, *i*, and *j* as diameters the length ranges of the semicircle or *l* are found using

$$C = D\pi \text{ (Eq. 4)}$$

$$l = \frac{C}{2} \text{ (Eq. 5).}$$

The value ranges of *l* can be calculated to afford a length range of ~7.22-17.6 Å (Table 1). This data was used in ligand design as it pertains to optimal ligand length ranges. Optimal length would be necessary to achieve maximum structural similarity between on particle presentation and the native antibody. The lengths of the sequences in (Å) were calculated using the bond lengths bonds between amino acids.

Table 1. Geometric Calculations of AuMPC parameter ranges.

Vertex-to-Vertex	Edge Length (nm)	*l* (Å)
Square edge (*a*)	0.46-0.56	7.22-8.79
Square diagonal (*b*)	0.66-0.80	10.4-12.5
Hexagon (*i*)	0.80-0.98	12.5-15.4
Hexagon (*j*)	0.92-1.12	14.4-17.6

The 8F8, 8M2, and 2G1 sequences were calculated to be ~21 Å, ~38 Å, and ~38 Å respectively. The 8F8 sequence is similar in length to *j* and would adopt nearly semicircular conformation if place-exchange occurred on the **same** hexagonal face. Longer sequences such as 8M2 and 2G1 are long enough to place exchange at vertex sites that are not contained on the same face or would adopt a flatter conformation assuming our PEG is rigid and can change angular conformation from the normal.

Ligand Design

The ligands designed were linear (LN) and looped (LP) peptidic 3-component systems. The 3-component ligand contains a surface modulator (connecting), spacing module (presentation), and an MRE (binding), inspired by the amino acids that were determined to be in the RBD by X-ray crystallography (Figure 3). Gold-thiol bonding has been utilized for stable surface functionalization.[7, 26-30] To achieve this, we designed our ligand with terminal

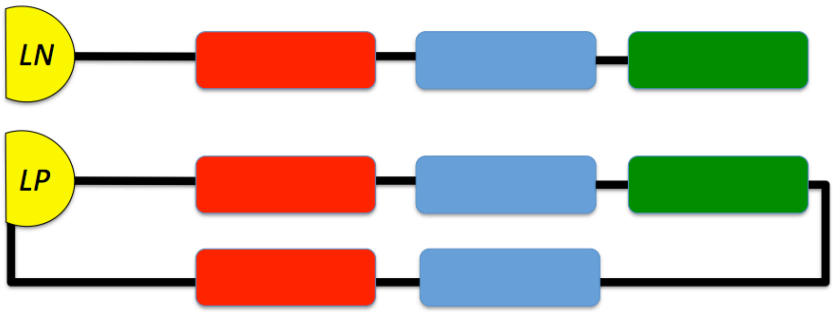

PLATFORM (Surface Chemistry)	Surface Modulator (Connector)	Spacing Modulator (Presentation)	Mol. Recog. Element (Binding)
Gold Nanoparticles (**MPC**) *LN*	Thiol	PEG	Peptide Sequence[1]
Gold Nanoparticles (**MPC**) *LP*	2 Thiols	2 PEGs	Peptide Sequence[1]

Figure 9. Linear and looped modular ligand design schematic detailing the surface modulation, spacing and molecular recognition element. Specific peptide sequence used for molecular recognition element determined by antibody sequencing and x-ray crystallography.

cysteine(s), which contains a thiol group, our surface modulator. Presentation of the CDR-H3 sequence away from the AuMPC surface is imperative and was considered in the design. The 3-component design uses a polyethylene glycol spacer unit that was synthetically incorporated into the ligand. This type of spacing module was imperative for tuning the distance and geometry of the ligand from the AuMPC by using discreet polyethylene glycol of different sizes. The MRE

of the 3-component system are the specific amino acid sequence of the CDR-H3 shown to be **in** the RBD as determined by Crowe and coworkers shown highlighted in (Figure 3).[36]

This ligand comes in two forms, mono- and bi-dentate. The mono-dentate design will have one surface modulator where as the bi-dentate will have two. This created either a mono-

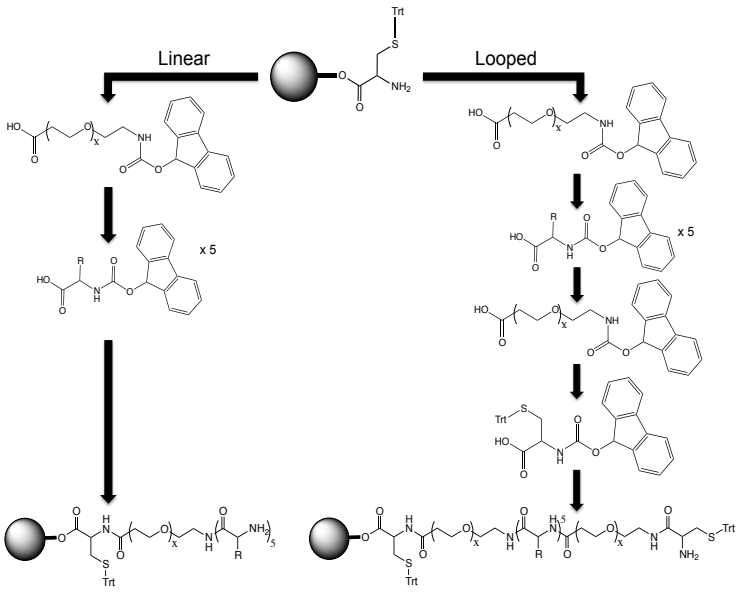

Figure 10. Standard FMOC solid-phase peptide synthesis pathways for linear and looped designs of the 8F8 and 2G1 sequences.

dentate linear ligand or a bi-dentate looped ligand that we presented on the AuMPC surface. The possibility of the bi-dentate ligand binding to two separate AuMPCs, creating a particle-to-particle linkage, was discussed and using strict control of concentration this was minimized and confirmed by TEM. The designed ligands were synthesized using standard FMOC solid-phase peptide coupling techniques.[31] Cysteine-based resin was used to incorporate a terminal thiol into the ligand design.

The mono-dentate ligand was built from the resin in the order of surface modulator, spacing modulator, terminating in the MRE (Figure 10). The bi-dentate or *looped* ligand was built from the resin in the order surface modulator, spacing module, MRE, spacing module,

terminating in another surface modulator (Figure 10). These ligands were purified via High Performance Liquid Chromatography (HPLC) and characterized using Matrix-Assisted Laser Desorption Ionization Mass Spectrometry (MALDI) and ^{1}H Nuclear Magnetic Resonance (^{1}H-NMR). The synthesized peptidic ligands were incorporated into the monolayer of the tiopronin by place exchange. These place-exchanged AuMPCs were purified by dialysis and characterized by ^{1}H-NMR.

The first aim was to design, synthesize and characterize a AuMPC-ligand antibody biomimetic. We achieved this by designing a synthetic mimic of the CDR-H3 of an antibody using peptide synthesis and coupled this with an AuMPC as a platform. More specifically, using interdisciplinary collaboration, we designed this AuMPC biomimetic to bind to the HA protein of the influenza virus.

Experimental

Chemicals:

Auric Acid (99%), Methanol (HPLC grade), N-(2-Mercaptopropionyl)glycine (tiopronin), and Sodium Borohydride were all purchased from Sigma Aldrich in the highest purity available. FMOC-Protected amino acids were purchased from AAPPTec. FMOC-protected polyethylene glycol spacers of various sizes were purchased from Quanta Biodesign. All other chemicals and solvents were used as received.

Synthesis:

In methanol (500 mL), Auric Acid $HAuCl_4 \bullet 3H_2O$ (Sigma Aldrich 99%) (1.00g, 2.5mmol) was dissolved and cooled to 0° C. N-(2-Mercaptopropionyl)glycine (tiopronin) (1.2

g, 7.5 mmol) was added to this solution and allowed to stir until ruby red solution turns clear. $NaBH_4$ (1.00 g, 25 mmol) was added quickly to the stirring solution while stirring vigorously at 0° C. Solution immediately went dark as the tiopronin monolayer-protected clusters are formed. The reaction is kept at 0° for 2 hours and then allowed to stir overnight at room temperature. Purification of the AUMPC suspension is achieved by rotary evaporation of the AuMPC-methanol suspension, resuspesion into DI H_2O with subsequent introduction into dialysis tubing (Thermo Scientific 10K-MWCO) and dialyzed against 4 L of DI H_2O for 4 days, changing the water twice a day. The AuMPC suspension is removed from the dialysis and the majority of DI H_2O is removed via rotary evaporation. The AuMPCs are then dried under a stream of N_2 in pre-weighed vials for yield calculations.

Characterization:

Images of the AuMPCs were taken on a Phillips CM20 Transmission Electron Microscope (TEM). 10 μL of a very dilute AuMPC solution were be dropped onto a TEM grid and allowed to air-dry overnight. TEM images at different magnification were taken to allow for size analysis of the AUMPCs. The TEM images were analyzed using ImageJ (NIH) and 400 different AuMPCs were analyzed for their diameter, giving rise to an average AuMPC size.

The chemical composition (organic/inorganic) of the AUMPCs was determined using an Instrument Specialist's TGA-1000 Thermogravimetric Analyzer (TGA). A small amount (approx. 10-15 mg) of dry AuMPCs were put into a pan that is then tared within the instrument and the furnace heats the sample from 25° C to 800° C. The mass loss from H_2O and organic tiopronin ligands were measured and that mass is represented by a percent mass. ^1H Nuclear Magnetic Resonance (NMR) spectra were obtained on a Bruker 400 Mhz instrument. A mixture of DI H_2O:D_2O (90:10) was used as the solvent. A small amount of AUMPCs were dissolved in this solvent for analysis. Spectra were taken using the pulse program *dhwatergate* to suppress

the H_2O proton signal and 600 scans were taken. UV-Visible absorption spectra were obtained on a Biotek Synergy H4 Hybrid Reader. The absorption spectra of the AUMPCs were taken in DI H_2O from 200-800 nm.

Peptide Synthesis:

Fmoc-Cysteine Wang Resin (0.1 g, 63 μmol of NH) (AAPPTec inc.) was introduced to a clean fritted peptide synthesis vessel. The resin was wetted with dichloromethane and allowed to swell for 10 minutes. The resin was then washed 3 times in the order dimethylformamide (DMF), methanol (MeOH) and DMF. The resin was then deprotected for 30 minutes using a 20% (v:v) mixture of piperidine and DMF, and then washed using the same wash procedure. The fmoc-PEG_8-Acid (Quanta Biodesign) (.125 g, 189 μmol) was dissolved in a small volume of DMF, then HOBT (0.03 g, 189 μmol), HBTU (0.07 g,189 μmol), and DIEA (65 μL, 378 μmol) were added to the Fmoc-PEG_8-Acid in DMF and then incubated with the deprotected resin for 2 hours. These steps are repeated for the introduction of each spacing modulator and amino acid needed. After the final amino acid is incorporated the resin is deprotected and then dried for cleavage. The peptide is cleaved from the resin at the C-terminus Cysteine using reagent K, a mixture of (trifluoroacetic acid:anisole:2,2-ethanedithiol:thioanisole) (90:5:2:3) by volume. After 2 hours of cleaving the solution of reagent K/peptide is filtered away from the resin and introduced to cold diethyl ether to precipitate the peptide. The solid peptide is pelleted using centrifugation and the solid peptide is washed 3 times with aliquots of cold diethyl ether, spun down, diethyl ether decanted and then allowed to dry. The crude peptide is then dissolved in a 80:15:5 mixture of H_2O:acetonitrile:glacial acetic acid then frozen and then lyophilized. The crude peptide is then dissolved in same mixture for high performance liquid chromatography purification. The peptide was purified on a Waters 4000 Semi-Prep HPLC system using a C18

column using a gradient of H_2O to acetonitrile. The fractions of interest were then collected, frozen and lyophilized to afford the powdery peptide.

Characterization:

The purified peptides were mass characterized using a Voyager Biosystems MALDI-MS instrument in positive or negative mode using Alpha-cyano as a matrix. The ^1H NMR spectra of the purified peptides were taken on a Bruker 400 Mhz instrument using D_2O.

Place Exchange Reactions and Synthesis:

Place exchange reactions were performed according to previous literature.[25] The purified cysteine-terminated peptides were be used to functionalize the tiopronin-gold AUMPCs (Figure 10). Ligands were dissolved in DI H_2O (10 mL) and incubated with a ratio of 1:25 ligands to tiopronin surface ligands for 3 days. The resulting solutions were then subjected to dialysis using 10 K MWCO tubing against DI H_2O for 3 days changing the water twice a day. The AuMPCs were dried by lyophilization.

Characterization:

The purified peptide functionalized AUMPCs were characterized as previously described using TEM, TGA, ^1H NMR, and UV-Vis. The TGA data coupled with the ^1H-NMR will provide us with an empirical formula for the functionalized AuMPCs in the form $Au_xTio_y(MRE)_z$. The protons associated with the tyrosine residues downfield in the NMR spectrum were used for qualitative and quantitative analysis of these AuMPCs.

Tiopronin Gold Monolayer-Protected Clusters

As described previously, a 1.00g batch of tiopronin gold AuMPCs were synthesized. The AuMPCs were made with a yield of %53. The characterization data was compiled and this was

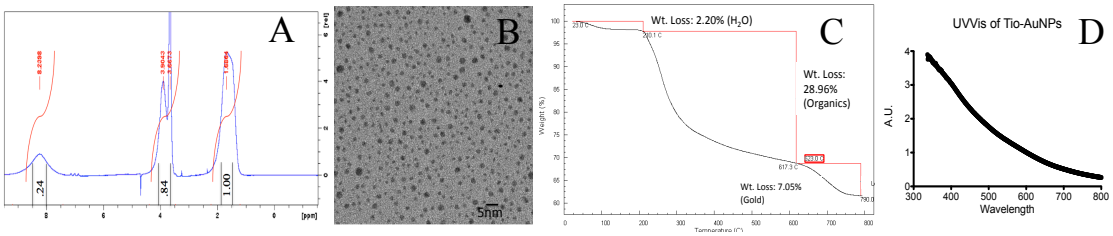

Figure 11. (A) NMR spectra of purified tiopronin-AuMPCs in D_2O, (B) TEM image of tiopronin-AuMPCs, (C) TGA graph of tiopronin-AuMPCs, (D) UV-Vis spectrum of tiopronin-AuMPCs.

used to determine the purity, average size of the AuMPCs, and the chemical composition.

The average size of the AuMPCs were 3.03±.37nm as determined by TEM (Figure 11). The organic composition of the AuMPC's was determined to be 28.96% by TGA, the %Au is calculated as 100% minus the percent organic or (100 - %organic) (Figure 11). Using the average size of the AuMPC, the occupancy of Au in face-centered cubic, and average bond radius for Au-Au the empirical formula for the AUMPCs can be achieved mathematically. The formula for tio-AuMPCs is in the form Au_xTio_y. The synthesized AuMPCs were calculated to have an average formula of $Au_{620}Tio_{382}$. The ^1H NMR (Figure 11) exhibits broad peaks, unlike normal solution NMR. The 4 different peaks shown in the NMR (1.67 ppm, 3.66 ppm, 3.84 ppm, 8.16 ppm) are associated with the 7 protons of the tiopronin ligand. The three methyl protons are shown at (1.67 ppm), the two protons of the methylene at (3.66 ppm), the single

proton at (3.85 ppm), and the secondary amine proton (8.16 ppm). The line broadening is due to the suspension nature of the tio-AuMPCs, the entire ligand on the surface is not soluble in the solvent and therefore does not behave as it would a free ligand in solution. Therefore the lack of dipolar coupling, leads to the broadness of the peaks. The lack of sharp peaks elsewhere in the spectra confirms the lack of impurities. Thermogravimetric analysis data was analyzed using the Instrument Specialist's software. The decline in mass percentage shown in the TGA graph (Scheme 11) is due to the "burning off" accomplished by the heating of the furnace. The first small decline ~2% at 100°C is attributed to loss of H_2O. The large decline that starts around 200°C and is completed around 620°C is attributed to the loss of tiopronin ligands on the AuMPC surface. This decline is what was used to calculate the %Organic associated with the AUMPCs. The last decline is thought to be associated with loss of actual Au atoms. The UV-Vis spectrum shown in (Figure 11) is used to confirm a small size of AUMPCs. The featureless decay coupled with the lack of a plasmon resonance band (520nm) confirms that the AUMPCs are smaller than 5nm.

Peptide Synthesis, Purification, and Characterization

The linear peptides were isolated and purified using standard protocols and the white powdery peptide was then characterized to confirm structure. MALDI-MS and ^{1}H-NMR spectra were collected and used for identity confirmation (Figure 12). For MALDI-MS experiments a small amount of peptide was dissolved and spotted on the instrument plate and then matrix spotted in the same well, after drying MALDI-MS spectra were collected. ^{1}H-NMR spectra were collected on a 400MHz instrument in D_2O. Synthesis of the looped peptide sequences proved difficult due to several reasons. The solubility profile of the PEG_x dominated the characteristics of the molecule and isolation and subsequent purification was affected. HPLC profiles of these

pegylated-looped molecules were markedly different from linear sequences of the same type. MALDI-MS spectra of HPLC fractions of the looped ligands did not afford m/z's consistent with the structure. Special consideration should be taken when synthesizing these looped ligands in the future due to the expensive nature of the PEG and the purification difficulties. Three peptides

Table 2. Successfully synthesized place-exchanged AuMPCs. Sequence associated with each listed along with empirical formula.

AuAUMPC	Sequence Presented	$Au_xTio_yMRE_z$
C-PEG_4-2G1	C-PEG_4-ISGYSGW	$Au_{620}Tio_{382}(CPEG_42G1)_3$
C-PEG_8-2G1	C-PEG_8-ISGYSGW	$Au_{620}Tio_{376}$(C-PEG_8-2G1)$_9$
C-PEG_4-8F8	C-PEG_4-SGYSG	$Au_{620}Tio_{350}$(C-PEG_4-8F8)$_{35}$

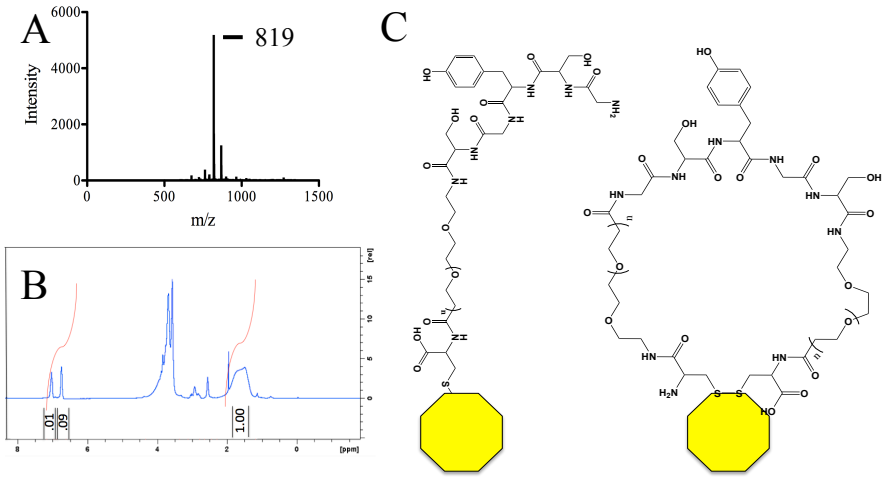

Figure 12. (A) MALDI-MS of C-PEG_4-8F8 after HPLC purification. Major peak at 819 *m/z* corresponds to the pure peptide. (B) ^{1}H-NMR of tiopronin-AuMPCs after place exchange with C-PEG_4-8F8. Tiopronin peaks present, and signature tyrosine peaks are visible at approximately 6.8 ppm and 7 ppm. (C) AuMPC schematic functionalized with one linear and looped ligand each (not drawn to scale).

were successfully purified and structure confirmed via MALDI-MS and ^{1}H-NMR (Table 2). These ligands were proper candidates to move forward with and place-exchange reactions were completed using these ligands.

Place-Exchange Reactions

After the characterization of the AuMPCs the place exchange reactions were completed using the synthesized and characterized ligands (Table 2). Failure to isolate pure peptide based from all of the designed linear and looped peptides caused us to move forward with only 3 successfully made peptides. The various 8F8 and 2G1 place exchanged AuMPCs were purified via dialysis and lyophilized to provide us with our AuMPCs now functionalized with our modular ligands and therefore signifying the completion of the second half of our first aim (Figure 12). The amount of place exchange achieved on each separate AuMPC was analyzed via ^{1}H NMR and the empirical formula was determined and is reported in the form $Au_xTio_yMRE_z$ (Table 2). We postulate that the differences seen in the amount of peptide exchanged for each linear sequence is directly related to structure and characteristics of the amino acid portion of our ligand. Although the 2G1 and 8F8 sequences are similar, the bulkiness of the isoleucine and tryptophan coupled with their more organic character lead us to believe that sterics and solubility directly impacted the lower place exchange efficiency. The longer PEG_8 linker presents the 2G1 peptide sequence further away from the tiopronin-monolayer on the surface and allows for more efficient place-exchange and higher substitution than the PEG_4 version of the same ligand. The presentation of the MRE on the surface of the can be tuned using the modular ligand design, or alternative platforms such as other size options of gold nanoparticles. The use of colloidal gold nanoparticles (AuNP) of different sizes could be used to further tune the presentation and packing ability of our linear and looped ligands. 7nm Tannic Acid-capped and 15nm citrate-

capped AuNPs are alternative platforms. These type of AuNPs can be easily functionalized through the thiol present in our ligand, and purification can be done by centrifugation and washing. UV-Vis spectroscopy is the most important characterization technique for colloidal AuNPs from 5-200nm. The plasmon resonance at approximately 520nm associated with 7nm and 15nm AuNPs can be used to confirm if the particles are aggregated as well as if they are functionalized with our ligand. The broadening of the plasmon band is indicative of aggregation, and a red shift (longer wavelengths) of the plasmon band is indicative of the change in the surface characteristics after the ligand is placed on the AuNP. This is confirmation that our ligand has been attached to the AuNP. Future research should strongly consider experimenting with different size regimes of particles to tune the ligand packing and conformation.

Conclusions

Interdisciplinary approaches to research are currently an effective method for attacking complex scientific questions. We have taken a problem, applied interdisciplinary methodology, and reported the synthesis of an AuMPC biomimetic based on the CDR-H3 of an antibody to pandemic influenza strains. The synthesis of these AuMPCs can be modified easily to afford any size range of clusters desired, and retaining the ability to place-exchange any ligands of interest into the monolayer with our surface modulator. Synthesis and characterization of modular peptides inspired by CDR-H3s completes our first aim and prepares AuMPCs to move forward to conduct binding studies.

Chapter III

BINDING EXPERIMENTS USING RECOMBINANT HEMAGGLUTININ

Introduction

Principles of Bio-layer Interferometry

The second aim to this research was to determine binding of our synthesized AuMPC biomimetic to the viral surface protein HA to which is was designed. When determining an experimental technique to test this binding Bio-layer interferometry became an attractive method. Experimental techniques such as Enzyme-Linked Immunosorbent Assay (ELISA), and QCM were considered for this aim due to their reliable nature and lab precedence respectively. Ultimately BLI emerged as the experimental technique that would afford us the sensitivity, parameter control, and non-destructiveness that we deemed necessary for our research. BLI, a technique developed by ForteBio for analysis of biomolecule interactions without the need for labeling, proved to be a more straightforward approach than ELISA and QCM.[32, 33] This technology can be used with analytes of 150Da or greater and our biomolecules of interest, as well as AuMPC are far greater than this mass. The principle of optical interferometry lies in the interaction of light waves with one another. Constructive or destructive interference is achieved by waves in phase or out-of-phase respectively. BLI technology employs this basic phenomenon in their fiber optic sensors for the signal. Within the fiber optic tip there is an internal reference and the change in reflectivity of white light shining down the tip will return waves of light from two different surfaces, the internal reference and the edge of the tip introduced to the solution.

A biomolecule of interest (small molecule, protein, etc.) can be immobilized on this sensor for "dip stick" type measurements. After immobilization of a biomolecule there is a change in the

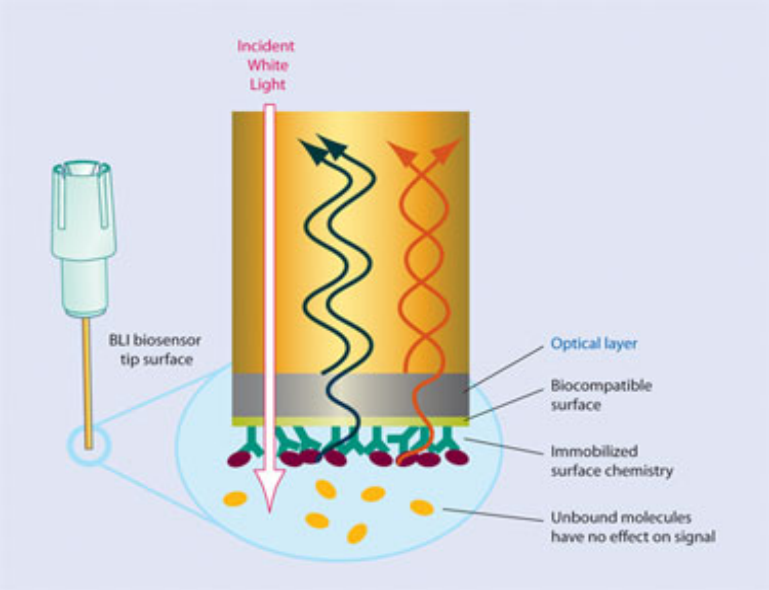

Figure 13. Bio-Layer interferometry schematic, showing the sensor, surface, and fiber optic layout.

optical thickness at the tip, which leads to an increase in path length of the reflection and change in the interference pattern. This shift in the interference pattern across the visible spectrum can be plotted as a magnitude over time and association curves are created. As biomolecules dissociate from the tip the interference pattern shifts back and this magnitude is also plotted as a magnitude over time, creating a dissociation curve. This process creates real-time kinetics and affinity measurements. The advantage of this technique is that this shift is only associated with molecules **bound** to the sensor (Figure 13). The Octet Red has multiplex and high throughput ability; experiments can be conducted in 96 well plates using a row of 8 separate sensors. This experiment also does not need large amounts of sample (200 µL), which works for small volumes of AuMPC solutions. The Octet has disposable streptavidin sensors that are easily

functionalized with our protein of interest HA via biotinylation. The model experiment with this instrument done by Abdiche and coworkers used commercially available monoclonal antibody "4901" with the antigen calcitonin gene-related peptide (CGRP).[32] They designed direct binding experiments, immobilizing 4901 on the octet sensor and binding CGRP this experiment showed precedence to use the Octet BLI systems for our experiments. The Octet system was also shown to be successful in detecting low affinity antibodies, which was also considered to be a positive quality of the technique.[33,34] Given the large nature of our AuMPC (~20 kD), we did not anticipate sensitivity issues as seen with smaller analytes.

Kinetic Basics

The picture of binding between two biomolecules where one is a ligand [A] and one is an immobilized protein [B] is modeled by mass action theory. This type of reaction between A and B are assumed to follow pseudo first-order kinetics and using the reaction equation

$$[A] + [B] \rightleftharpoons [AB] \text{ (Eq. 6).}$$

The forward, association phase of the protein-ligand complex [AB], results in an increase in [AB] over time. Where k_f is the forward rate constant, and k_r is the reverse rate constant. Taking the derivative of (Eq. 6) in respect to t gives a differential rate equation that relates the various parameters k_f and k_r to the concentrations of [A], [B] and [AB]

$$\frac{d[AB]}{dt} = k_f[A][B] - k_r[AB] \text{ (Eq. 7).}$$

At t=0 no [AB] is formed, but at some time t the amount of [B] is equal to the initial concentration of biomolecule, $[B]_o$ minus the concentration of [AB] formed. Plugging that relationship into (Eq. 7) affords us

$$\frac{d[AB]}{dt} = k_f[A]([B]_o - [AB]) - k_r[AB] \text{ (Eq. 8).}$$

This differential equation describes the formation of the [AB] complex in terms of [A] and $[B]_o$ where k_f is the forward rate constant which describes the rate of formation of the complex in units $M^{-1}s^{-1}$. The stability of the [AB] complex formed is determined by the rate constant k_r in units s^{-1}. In the case of bio-layer interferometry our protein of interest [B] is immobilized on the sensor tip and the AuMPC in solution is assumed to be a constant [A]. AuMPC concentration is considered to be constant because the amount of [B] immobilized on the surface is a very small amount, even if all the immobilized [B] was used in formation of [AB] the concentration of AuMPCs used would be ~10^{-15} in quantity. Therefore [A], $[B]_o$ and [AB] can be expressed in terms of response or R by substitution of concentration C*, and R_{max} into (Eq. 8)

$$\frac{dR}{dt} = k_f C^*(R_{max} - R) - k_r R \text{ (Eq. 9)}$$

The differential equation in terms of R was built by substituting [A] with the term C* for concentration constant and R_{max}, the maximum response due to total amount of immobilized protein $[B]_o$, and at any time t, (R_{max} – R) is equal to the unoccupied surface protein. Rearrangement of (Eq. 9) gives

$$\frac{dR}{dt} = k_f C^* R_{max} - \left(k_f C + k_r\right)R \text{ (Eq. 10)}$$

Linear transformations from (Eq. 10) can be done to determine values of k_f and k_r but transform errors in the primary data.[37] This fact has moved researchers to use the integrated rate equation which allows direct analysis of the data written as

$$R_t = \frac{k_f C^* R_{max}[1-e^{-\left(\left(k_f C + k_r\right)t\right)}}{C k_f + k_r} \text{ (Eq. 11).}$$

This kinetic explanation of protein-AuMPC interaction with 1:1 stoichiometry leads to the prediction of Langmuirian behavior for the adsorption, and desorption events. The Langmuir absorption model is standard mathematical model for quantification of molecule absorption to a surface. Langmuir isotherms can be used with inherent assumptions of surface site equivalency, monolayer coverage at these surface sites, and no interactions between adsorbed molecules at adjacent surface sites. The BLI experiment we have designed fits within the realms of these assumptions. The surface of the fiber optic tip is functionalized with HA protein that are assumed to be equivalent. The binding anticipated, due to the mimicry CDR-H3's interaction in the RBD, is 1:1. Due to the low concentration of actual bound protein to the fiber optic tip we don't expect interaction between two adsorbed AuMPCs with one another.

In our experiment HA protein was immobilized on the sensors using standard biotinylation and introduction to the streptavidin sensors and these sensors were subsequently introduced to each different AuMPC biomimetic synthesized as well as reference antibody.

Experimental

Chemicals

The Crowe Lab at Vanderbilt University provided the specific H2N2 HA protein (A/Japan/305/1957) and the Anti-H2N2 antibody (8F8). AuMPCs that were used were synthesized as previously described. Phosphate buffered saline 1X (PBS) was purchased from (Life Technologies). Polyoxyethylenesorbitan monolaurate (TWEEN 20) and bovine serum albumin (BSA) were purchased from Sigma Aldrich. EZ-Link Biotin N-hydroxysuccinimide ester (NHS) and Biotin-PEG_2 were purchased from Thermo Scientific. Streptavidin (SA) sensors were purchased from ForteBio. Standard Black propylene flat bottom 96-well 200μL plates were used for all experiments. Deionized water was purified using a Modulab Water Systems unit (~18 MΩ).

Biotinylation of HA

The HA (A/Japan/305/1957) was biotinylated using EZ-Link Biotin-NHS procedure. The biotinylated HA (Biotin-HA) was used for all subsequent binding experiments.

Titration of Anti-HA (8F8)

The 8F8 antibody was titrated against HA (A/Japan/305/1957) using the ForteBio Octet RED96 with standard black flat-bottom 96-well plates. Concentrations of 8F8 antibody ranging from 600 μM to 50 μM in 1X PBS were used for the titration. SA sensors were soaked prior to use for 5 minutes in 1X PBS buffer. All subsequent experimental steps were done in 1X PBS buffer. A 2-minute baseline step was conducted followed by a 2 minute loading step where biotin-HA was bound to the tip. After loading a 1-minute wash step was done post loading. A 2 minute binding using a biotin-PEG_2 was completed as a blocking step to bind any exposed SA and minimize

non-specific interactions. A 2 minute wash step followed the blocking, and then a 5 minute binding step (association) of 8F8 antibody was completed. A 5 minute dissociation step into buffer was then completed signifying the completion of the antibody titration experiment. The concentration of antibody in the titration that achieves ~0.5 nm binding interference shift is the optimal concentration to use in subsequent experiments.[33] 200μM Biotin-HA was used for all subsequent experiments. The antibody-antigen binding affinity was calculated using ForteBio Octet Data Analysis software.

Double-Referenced Binding Studies of Antibody Mimic AuMPCs

Three different AuMPCs were used for indirect binding studies with HA (A/Japan/305/1957). The different AuMPCs tested were each separately dissolved in buffer at surface ligand concentration 300mM and 100mM respectively, and placed in separate binding columns in the 96-well plate. SA sensors were soaked prior to each experiment in 1X PBS buffer with .2% TWEEN and .01% BSA for 5 minutes. This buffer was also the buffer used for all double-referenced binding studies. Binding studies were conducted in the order soak>wash>binding>dissociation and this data was subtracted from the data collected for the same AuMPCs in the order soak>load>wash>binding>dissociation (Figure 14). All steps were done at 1000rpm. One well in each binding column was filled with buffer only as a blank, one well in each binding column had 8F8 antibody at 0.8×10^{-9}M as our reference. The rest of the wells in the binding column were filled with the AuMPCs of interest. The association-dissociation curves obtained were fitted globally using 1:1 Langmuir model. The fitting was done using the ForteBio Data analysis software to obtain the k_f, k_r, K_a, K_D.

Binding Experiment and Data Analysis

After the synthesis and characterization of linear and looped AuMPC based off of the MRE of 2G1, and 8F8 antibodies binding studies were conducted. This was a novel application of such instrument; currently there is no literature precedence for BLI for protein-MPC interactions. ForteBio's bio-layer interferometry technology proved to be an effective approach to determine if our AuMPC biomimetic can bind antigenic protein. The double referencing was used to subtract out any non-specific binding of our AuMPC to the SA tip. To achieve double-referencing a dummy-load step was incorporated into the experiment. The SA sensors in this

Table 3. Equilibrium association and dissociation constants for 8F8 and 2G1 place-exchanged AuMPCs, data for two concentrations of AuMPCs. *Error less than 0.01.

AuMPC	K_a (x 10^6 M^{-1}) 0.1M	K_a (x 10^6 M^{-1}) 0.3M	K_D (x 10^{-6} M) 0.1M	K_D (x 10^{-6} M) 0.3M
C-PEG$_4$-2G1	1.2 ± 0.08	0.17 ± 0.01	0.9 ± 0.1	6.0 ± 0.4
C-PEG$_8$-2G1	15 ± 3.1	0.1*	0.1 ± 0.01	14.0 ± 0.8
C-PEG$_8$-8F8	9.7 ± 2.4	0.7 ± 0.1	0.1 ± 0.03	1.4 ± 0.3

case were introduced to buffer only during the load step and contained no HA on the sensor and data was collected then washed in buffer. The unloaded sensors were then introduced to the AuMPC solutions and data was collected for 15 minutes. The AuMPC bound sensors were then introduced to buffer in the dissociation column and data was collected for 15 minutes. The lack

of HA protein on the SA tip creates a reference for the software to subtract out non-specific binding and create truer binding curves for the AuMPCs. The curves for the double referenced experiment were globally fit using a 1:1 Langmuir model.

The experimentally determined dissociation constants K_D for the three functionalized AuMPCs range from $0.1x10^{-}$M to $14x10^{-6}$M (Table 3). The experimentally determined association constants K_a range from $0.1x10^{6}M^{-1}$ to $15x10^{6}M^{-1}$. Therefore our AuMPC biomimetic does not bind HA as tightly as the native 8F8 antibody with K_D on the order of $1x10^{-9}$M. This data correlates with literature precedence of biomimetic AuMPCs. Work by Gerdon

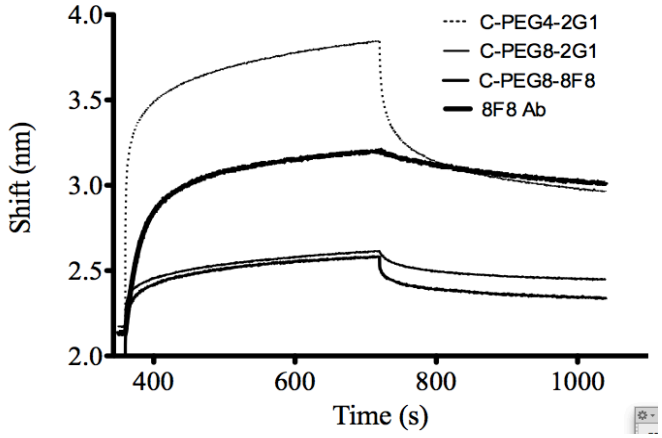

Figure 14. Double-referenced bio-layer interferometry experiment curves using 8F8 and 2G1 AuMPCs compared to 8F8 antibody.

produced a K_D value of $.17x10^{-6}$M and K_a $9x10^{6}M^{-1}$ for AuMPC-protein binding using QCM.[8] Analysis of the preliminary data shows that there is vast room for experimental improvement. The K_a within our experiment was shown to increase with decrease in concentration, most likely due to slower AuMPC association with the tip due to bulk concentration behavior. Widening the concentration range of the AuMPCs tested to 10^{-6}-10^{-9}M will give insight into concentration

dependency on signal. Looped presentation AuMPCs will afford a comparison from the linear sequence. We believe the conformational presentation of the peptide sequence will have implications on the association and dissociation constants. There is also synthetic territory that has not been charted, such as anchored peptide sequences of complete CDR-H3s. These are much longer sequences than the ones studied. This could give rise to favorable interactions of the peptide with HA **outside** of the RBD. Considering the complex nature of this experiment revisiting the assumptions listed previously would also be warranted. Line fitting parameters R^2 and X^2 are a measure of the quality of fit. With R^2 values of 0.77-0.92 and X^2 values of 0.03-0.61 steps should be taken to improve both of these parameters. We used the standard 1:1 model but given the novelty and complexity of this type of experiment other fitting models should be considered and tested. The mass-transfer model is used in situations where the ligand is first transferred from bulk solution to the sensor interface, and then binding to the protein on the sensor surface occurs. The diffusion of the ligand from the bulk solution to the sensor is a slower process than the binding of the ligand to the sensor creating a lower concentration at the sensor surface. This could be the case with our AuMPCs that have a very large MW and potentially slow diffusion from bulk solution and the coefficient of mass transfer k_t would be used. There is also a model for the case of the bivalent analyte. We initially made the assumption that we have only one AuMPC binding per HA due to the surface concentration of HA. These AuMPCs have multiple ligands on the surface and just as the case of an antibody that has two ligands per one structure this assumption may not hold true. One AuMPC could potentially bind two different HA proteins at the sensor surface. In the case of concentrated solutions such as ours this effect has been seen. Two separate k_f values arise where the second is much more difficult to interpret because the first binding event shifts the equilibrium of the system. The envelope glycoprotein, gp120, of human immunodeficiency virus is the surface protein responsible for viral entry into cells much like HA to influenza. The utilization of a

negative control viral protein such as gp120 with BLI experiments would further determine specificity of the AuMPCs. Ultimately, testing our probe against all HA subtypes would determine if the CDR-H3 sequences are broadly neutralizing when presented by AuMPCs.

Conclusions

Experiments described previously have brought forth preliminary data of CDR-H3 mimic AuMPCs interaction with HA using BLI. We successfully assembled and characterized these AuMPCs and used them to bind the HA protein influenza. The results of these binding experiments suggest that these AuMPCs bind the HA protein to varying degrees. The results also suggest that the design and components of these nanoscale probes were both important in eliciting biological activity in the form of cluster-protein interaction. Biological activity of these novel AuMPCs was determined to be on the scale of previous research using alternative methods. This research describes the first steps in designing and optimizing bioinorganic antibody mimics using AuMPCs. Using this foundation, future endeavors in this research will optimize kinetic data fitting to better understand the AuMPC-HA interaction and provide a basis for studies of conformational replicas of CDR-H3s on a tunable cluster surface.

REFERENCES

1. Frens, G., CONTROLLED NUCLEATION FOR REGULATION OF PARTICLE-SIZE IN MONODISPERSE GOLD SUSPENSIONS. *Nature-Physical Science* 1973, 241, 20-22.

2. Turkevic.J; Demirci, S.; Skvir, D. J., INTERACTION OF COLLOIDAL PARTICLES WITH SURFACES OF BIOLOGICAL SIGNIFICANCE. *Croatica Chemica Acta* 1973, 45, 85-96.

3. Cardinal, J.; Klune, J. R.; Chory, E.; Jeyabalan, G.; Kanzius, J. S.; Nalesnik, M.; Geller, D. A., Noninvasive radiofrequency ablation of cancer targeted by gold nanoparticles. *Surgery* 2008, 144, 125-132.

4. Cliffel, D. E.; Turner, B. N.; Huffman, B. J., Nanoparticle-based biologic mimetics. *Wiley Interdisciplinary Reviews-Nanomedicine and Nanobiotechnology* 2009, 1, 47-59.

5. Jayagopal, A.; Halfpenny, K. C.; Perez, J. W.; Wright, D. W., Hairpin DNA-Functionalized Gold Colloids for the Imaging of mRNA in Live Cells. *Journal of the American Chemical Society* 2010, 132, 9789-9796.

6. Sun, I.-C.; Eun, D.-K.; Na, J. H.; Lee, S.; Kim, I.-J.; Youn, I.-C.; Ko, C.-Y.; Kim, H.-S.; Lim, D.; Choi, K.; Messersmith, P. B.; Park, T. G.; Kim, S. Y.; Kwon, I. C.; Kim, K.; Ahn, C.-H., Heparin-Coated Gold Nanoparticles for Liver-Specific CT Imaging. *Chemistry-a European Journal* 2009, 15, 13341-13347.

7. Templeton, A. C.; Chen, S. W.; Gross, S. M.; Murray, R. W., Water-soluble, isolable gold clusters protected by tiopronin and coenzyme A monolayers. *Langmuir* 1999, 15, 66-76.

8. Gerdon, A. E.; Wright, D. W.; Cliffel, D. E., Hemagglutinin linear epitope presentation on monolayer-protected clusters elicits strong antibody binding. *Biomacromolecules* 2005, 6, 3419-3424.

9. Miller, S. A.; Hiatt, L. A.; Keil, R. G.; Wright, D. W.; Cliffel, D. E., Multifunctional nanoparticles as simulants for a gravimetric immunoassay. *Analytical and Bioanalytical Chemistry* 2011, 399, 1021-1029.

10. Webster, R. G.; Bean, W. J.; Gorman, O. T.; Chambers, T. M.; Kawaoka, Y., EVOLUTION AND ECOLOGY OF INFLUENZA-A VIRUSES. *Microbiological Reviews* 1992, 56, 152-179.

11. Kilbourne, E. D., *The Influenza Viruses and Influenza*. Academic Press Inc.: 111 Fifth Avenue, New York, New York 10003, 1975.

12. Patterson, S.; Oxford, J. S.; Dourmashkin, R. R., STUDIES ON THE MECHANISM OF INFLUENZA-VIRUS ENTRY INTO CELLS. *Journal of General Virology* 1979, 43, 223-229.

13. Nabel, G. J.; Wei, C.-J.; Ledgerwood, J. E., Vaccinate for the next H2N2 pandemic now. *Nature* 2011, 471, 157-158.

14. Stoehr, K., Vaccinate before the next pandemic? *Nature* 2010, 465, 161-161.

15. Arruebo, M.; Valladares, M.; Gonzalez-Fernandez, A., Antibody-Conjugated Nanoparticles for Biomedical Applications. *Journal of Nanomaterials* 2009.

16. Asai, D. J., *Antibodies in Cell Biology*. Academic Press, INC.: 1250 Sixth Ave, San Diego, CA, 1993; Vol. 37, p 452.

17. Crowe, J. E. J., Human Monoclonal Antibodies to Pandemic 1957 H2N2 and Pandemic 1968 H3N2 Influenza Viruses. Vanderbilt University: 2012.

18. North, B.; Lehmann, A.; Dunbrack, R. L., Jr., A New Clustering of Antibody CDR Loop Conformations. *Journal of Molecular Biology* 2011, 406, 228-256.

19. Ambrosi, A.; Airo, F.; Merkoci, A., Enhanced Gold Nanoparticle Based ELISA for a Breast Cancer Biomarker. *Analytical Chemistry* 2010, 82, 1151-1156.

20. Cutler, E. C.; Lundin, E.; Garabato, B. D.; Choi, D.; Shon, Y. S., Dendritic functionalization of monolayer-protected gold nanoparticles. *Materials Research Bulletin* 2007, 42, 1178-1185.

21. Driskell, J. D.; Jones, C. A.; Tompkins, S. M.; Tripp, R. A., One-step assay for detecting influenza virus using dynamic light scattering and gold nanoparticles. *Analyst* 2011, 136, 3083-3090.

22. Eck, W.; Craig, G.; Sigdel, A.; Ritter, G.; Old, L. J.; Tang, L.; Brennan, M. F.; Allen, P. J.; Mason, M. D., PEGylated Gold Nanoparticles Conjugated to Monoclonal F19 Antibodies as Targeted Labeling Agents for Human Pancreatic Carcinoma Tissue. *Acs Nano* 2008, 2, 2263-2272.

23. Liu, H.; Malhotra, R.; Peczuh, M. W.; Rusling, J. F., Electrochemical Immunosensors for Antibodies to Peanut Allergen Ara h2 Using Gold Nanoparticle-Peptide Films. *Analytical Chemistry* 2010, 82, 5865-5871.

24. Mu, B.; Huang, X.; Bu, P.; Zhuang, J.; Cheng, Z.; Feng, J.; Yang, D.; Dong, C.; Zhang, J.; Yan, X., Influenza virus detection with pentabody-activated nanoparticles. *Journal of Virological Methods* 2010, 169, 282-289.

25. Hostetler, M. J.; Templeton, A. C.; Murray, R. W., Dynamics of place-exchange reactions on monolayer-protected gold cluster molecules. *Langmuir* 1999, 15, 3782-3789.

26. Hostetler, M. J.; Wingate, J. E.; Zhong, C. J.; Harris, J. E.; Vachet, R. W.; Clark, M. R.; Londono, J. D.; Green, S. J.; Stokes, J. J.; Wignall, G. D.; Glish, G. L.; Porter, M. D.; Evans, N. D.; Murray, R. W., Alkanethiolate gold cluster molecules with core diameters from 1.5 to 5.2 nm: Core and monolayer properties as a function of core size. *Langmuir* 1998, 14, 17-30.

27. Templeton, A. C.; Wuelfing, M. P.; Murray, R. W., Monolayer protected cluster molecules. *Accounts of Chemical Research* 2000, 33, 27-36.

28. Whetten, R. L.; Khoury, J. T.; Alvarez, M. M.; Murthy, S.; Vezmar, I.; Wang, Z. L.; Stephens, P. W.; Cleveland, C. L.; Luedtke, W. D.; Landman, U., Nanocrystal gold molecules. *Advanced Materials* 1996, 8, 428-&.

29. Chen, S. W.; Templeton, A. C.; Murray, R. W., Monolayer-protected cluster growth dynamics. *Langmuir* 2000, 16, 3543-3548.

30. Jadzinsky, P. D.; Calero, G.; Ackerson, C. J.; Bushnell, D. A.; Kornberg, R. D., Structure of a thiol monolayer-protected gold nanoparticle at 1.1 angstrom resolution. *Science* 2007, 318, 430-433.

31. LLC., a., Practical Synthesis Guide to Solid Phase Peptide Chemistry. p. 76.

32. Abdiche, Y.; Malashock, D.; Pinkerton, A.; Pons, J., Determining kinetics and affinities of protein interactions using a parallel real-time label-free biosensor, the Octet. *Analytical Biochemistry* 2008, 377, 209-217.

33. Li, J.; Schantz, A.; Schwegler, M.; Shankar, G., Detection of low-affinity anti-drug antibodies and improved drug tolerance in immunogenicity testing by Octet (R) biolayer interferometry. *Journal of Pharmaceutical and Biomedical Analysis* 2011, 54, 286-294.

34. Weetall, H. H., *Immobilized Enzymes, Antigens, Antibodies, and Peptides: Preparation and Characterization*. MARCEL DEKKER, INC.: 270 Madison Ave, New York, New York 10016, 1975; Vol. 1.

35. Influenza, W. H. O. C. C. f. R. a. R. o., Concepts and Procedures for Laboratory-based Influenza Surveillance. Centers for Disease Control and Prevention, Atlanta, GA.

36. Xu, Rui; Krause, Jens; McBride, Ryan; Paulson, James; Crowe Jr., James; Wilson, Ian, A recurring motif for antibody recognition of the receptor-binding site of influenza hemaggultinin. *Nature Structural Molecular Biology* 2013, 20, 363-370

37. O'Shannessy, Daniel, J; Brigham-Burke, Michael; Soneson, K. Karl; Hensley, Preston; Brooks, Ian, Determination of Rate and Equilibrium Binding Constants for Macromolecular Interactions Using Surface Plasmon Resonance: Use of Nonlinear Least Squares Analysis Methods. *Analytical Biochemistry* 1993, 212, 457-468